Development of Nanostructured SiC Coating on Advanced Carbon Materials and Their Applications†

MORISADA Yoshiaki* and MIYAMOTO Yoshinari**

Abstract

Diamond particles and multi-walled carbon nanotubes (MWCNTs) were coated with a nanometer-sized SiC polycrystalline layer by the reaction of SiO(g) and CO(g). The growth mechanism of SiC and the oxidation resistance of the SiC-coated carbon materials were studied. The growth process of the SiC layer can be separated into two steps. In the first step, a thin layer of SiC is formed due to the reaction between SiO vapor and carbon materials. In the second step, nanometer sized SiC granules are deposited on the SiC layer by the reaction between SiO vapor and CO. The oxidation resistance of the carbon materials was improved by the SiC coating. Oxidation of the SiC-coated diamond particles began at 950 ℃, which is 400 ℃ higher than that of uncoated diamond. MWCNTs were oxidized completely in air at 650 ℃ for 60 min. However, about 90 mass % of the SiC-coated MWCNTs remained after the same oxidation test. Dense composites reinforced by the SiC-coated carbon materials were successfully fabricated using a pulsed electric current sintering. The composites showed excellent mechanical properties compared to the monolithic materials and the composites reinforced by uncoated carbon materials.

KEY WORDS: (SiC coating), (Diamond particles), (MWCNTs), (Oxidation resistance), (Composites)

1. Introduction

Due to various bond-structures such as sp^3, sp^2, sp hybrids, and multiple p_π- p_π bonds, carbon can form 1-, 2-, and 3- dimensionally bond-structured substances and provide a wide-range of applications[1]. Carbon materials such as graphite, diamond, activate carbons, carbon fibers, and C-C composites have been extensively investigated and used for many years. Since the discovery of carbon nanotubes in 1997, carbon materials have been newly focused as frontier materials in various fields[2-15].

However, carbon materials have a serious shortcoming. They are easily oxidized above 530 ℃ in air. It is possible to protect graphite plates or carbon fibers with SiC coating by CVD or pyrolysis of polymers containing Si and C[16-18]. SiC is known as an effective material to prevent oxidation and corrosion due to the strong covalent bond and the passive-oxidation by forming a protective SiO_2 layer on SiC[19-24].

It is difficult, however, to coat fine carbon materials such as carbon nantubes and fine diamond powders with SiC uniformly. The SiC coating on carbon nanotubes would improve not only the oxidation resistance, but poor adhesion with matrix when they are used as nano-reinforcements. Many researchers indicate that the improvement of the adhesion between carbon nanotubes and matrix is a critical issue to improve the mechanical properties of their composites[25-27]. The SiC coating is very useful for fine diamond particles as well. Diamond is widely used for cutting, grinding, and polishing of various materials, however the graphitization of diamond by the reaction with transition metals such as iron, cobalt, and nickel limits its applications. If diamond particles could be coated with an effective protective layer, they could be used at high temperatures under the oxidizing and corrosive environments and the tool life could be extended. New composite formations of diamond with WC/Co would be possible.

In this paper, a new and easy process for producing SiC coatings on fine carbon materials is described[28-30] and some applications of the SiC-coated diamond particles and carbon nanotubes to create new composites are demonstrated[31-33].

2. Coating method of nanostructured SiC

2.1 Coating assembly

The SiC coating is produced by means of the reaction of SiO vapor and carbon materials. Commercial SiO powders (99.9 % pure) are provided as the silicon source. The carbon materials are placed on the SiO powder bed via carbon felt as illustrated in Fig. 1. This assembly is

† Received on January 31, 2004
* Graduate Student, Osaka University
** Professor

Transactions of JWRI is published by Joining and Welding Research Institute of Osaka University, Ibaraki, Osaka 567-0047, Japan

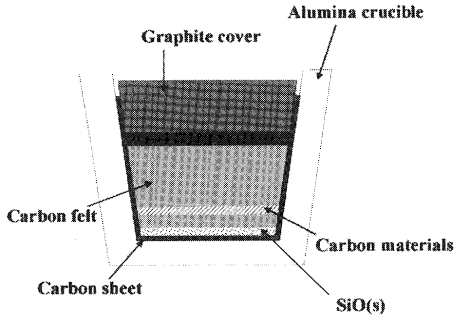

Fig. 1 Assembly for the SiC coating of carbon materials.

covered with carbon sheets in an alumina crucible to maintain the SiO gas pressure in the crucible and heated in a vacuum furnace at various temperatures from 1150 to 1550 ℃ in vacuum (about 0.03 Pa) for periods of time between 1 and 90 minutes. It is necessary to heat at a temperature greater than 1150 ℃ for the vaporization of solid SiO.

2.2 SiC Coating on diamond particles

Diamond powders with the particle size of 1 to 30 μm are used for the SiC coating. Figure 2 shows a TEM image of the SiC-coated diamond with the particle size of ~1 μm. Each diamond particle is completely covered with a polycrystalline SiC layer of ~60 nm thick. The

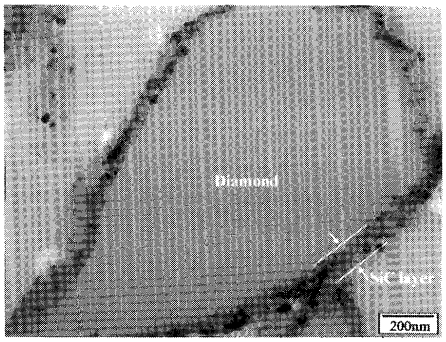

Fig. 2 TEM image of SiC-coated diamond particles.

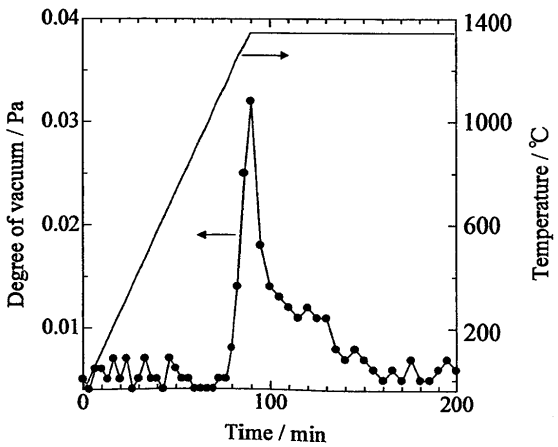

Fig. 3 Temperature and degree of vacuum in the furnace.

grain size of SiC is several nm. Though a large thermal expansion mismatch exists between SiC (α=4.6×10^{-6}/K) and diamond (α=3.1×10^{-6}/K), no cracking or debonding occurs in the SiC layer or at the interface. If there is gradual change in composition from diamond to SiC at the interface, the thermal stress would be relaxed.

Figure 3 shows the relation between temperature and pressure in the furnace when the assembly of SiO powders, carbon sheets and carbon felts is heated. The increase of the total pressure in the furnace at about 1200 ℃ results from the vaporization of SiO according to the reaction (1). The evolution of CO gas following the formation of SiC according to the reaction (2) causes the increase of the total pressure after vaporization of SiO[34-36]. In this case, the surface of carbon sheets and carbon felts should react and transform to SiC producing CO gas. Then, the diamond surface reacts with SiO(g) and forms a thin SiC layer on the diamond. This SiC layer will act as a protective layer to limit the reaction (2) from proceeding further and thus limiting the evolution of CO(g) from diamond.

$$SiO(s) \rightarrow SiO(g) \quad (1)$$

$$2C(s) + SiO(g) \rightarrow SiC(s) + CO(g) \quad (2)$$

The SiO vapor is consumed within 30 min under these treatment conditions. Further treatment over 30 min causes thinning of the SiC layer probably due to the active-oxidation taking place according to reaction (3). The partial pressure of oxygen in the furnace is about 6.0×10^{-3} Pa and this value at the coating temperature belongs to the active-oxidation region[37-40]. Oxygen is continuously supplied from the outer atmosphere.

$$SiC(s) + O_2(g) \rightarrow SiO(g) + CO(g) \quad (3)$$

The SiC-coated diamond particles can be characterized by X-ray powder diffractometry. The diffraction peak appears at 35.6°which is assigned as β-SiC (111) plane.

The mechanism of SiC coating on diamond can be analyzed as follows. When the SiC-coated diamond particles are placed in an alumina container and heated to 1200 ℃ in an air flow using a thermogravimetric apparatus, the sample weight decreases with increasing temperature mainly due to the oxidation of diamond and reaches minimum at about 1000 ℃ where diamond is almost completely converted to CO_2 gas leaving SiC behind. When it is further heated above 1000 ℃, the minimum weight increases slightly due to the passive-oxidation of the SiC layer. Because the mass gain due to the silica formation on SiC below 1000 ℃ is negligibly small, we can determine the minimum weight as the initial weight of the SiC layer on diamond. Let us consider a model structure consisting of a diamond sphere that is coated uniformly with SiC. Based on this model, the initial thickness of the SiC layer is expressed using the following equation.

$$W_f / n = 4\pi r_i^2 l \rho_{SiC} \quad (4)$$

where W_f is the minimum weight corresponding to the initial weight of the SiC layer, n is the number of diamond particles, r_i is the average radius of a diamond particle, l is the thickness of the SiC layer, and ρ_{SiC} is the density of SiC (3.2 g/cm^3).
The number of diamond particles can be obtained as follows.

$$n = (W_i - W_f) / 4/3\pi r_i^3 \rho_{dia} \quad (5)$$

where W_i is the initial weight of a SiC-coated diamond, and ρ_{dia} is the density of diamond (3.5 g/cm^3).
By substituting equation (4) into (5), the thickness (l) of the SiC layer is calculated using the following equation.

$$l = W_f r_i \rho_{dia} / 3(W_i - W_f)\rho_{SiC} \quad (6)$$

Figure 4 shows the calculated results of the thickness of the SiC layer and the mass gain due to the SiC formation depending on the coating temperature and time. The SiC coating for 90 min was obtained by repeating three times a 30 min coating. The thickness of the SiC layer increases with an increase in the coating time and temperature. The weight of the SiC layer increases linearly with time. This result suggests that the growth of the SiC layer is not controlled by the self-diffusion of Si or C atoms through SiC, but by precipitation or deposition of SiC from vapor phase reaction. The following vapor-solid reactions account for the linear growth of the SiC layer with coating time.

$$SiO(g) + 3CO(g) \rightarrow SiC(s) + 2CO_2(g) \quad (7)$$

$$CO_2(g) + C(s) \rightarrow 2CO(g) \quad (8)$$

Based on these analyses of the SiC coating, the growth mechanism of the SiC layer on diamond is considered as follows. In the early stage of the SiC formation on diamond, a very thin SiC layer is formed on the diamond surface according to reaction (2) between diamond and SiO(g). Once the SiC layer is formed, this reaction does not proceed further due to the protective layer of SiC. The carbon sheet and felt in an alumina crucible act as the carbon source. The reaction of CO_2(g) with these carbon sources will produce further CO(g) and deposit SiC(s) by reaction (7). Thin β-SiC whiskers are observed on the surface of the SiC-coated diamond, suggesting the vapor growth of SiC.

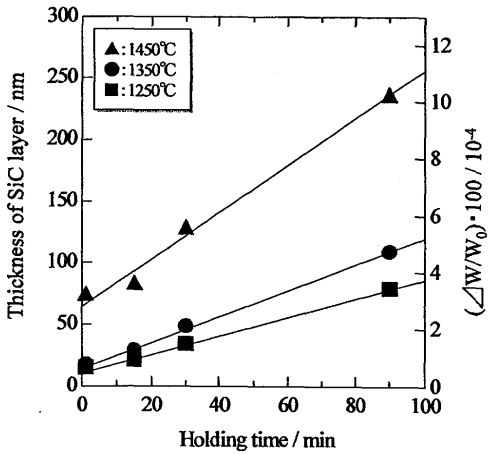

Fig. 4 Thickness and mass gain of the SiC layer on diamond particle.

The apparent activation energy of the SiC formation reaction is obtained from an Arrhenius plot of the rate constants that can be calculated using the mass gain data as a function of the coating temperature and using the least-square method. The calculated value is 100±21 kJ/mol. Shimoo et al. calculated the apparent activation energy for the formation of a SiC layer on a graphite plate based on reaction (7) and obtained 97 kJ/mol[36]. Both values show an excellent agreement.

Figure 5 shows SEM photographs of the surface of SiC-coated diamond particles coated at 1350 ℃. Tiny granules of SiC were deposited and aggregated with an increase in coating time. Even for samples treated for 1 min, the entire surface is considered to be covered with a thin SiC layer formed by the direct reaction of diamond and SiO(g) because the samples show good oxidation resistance as to be discussed later. EDX analysis shows a uniform distribution of Si atoms on the entire surface of the SiC-coated diamond particle.

Therefore, the SiC layer on diamond is considered to grow in a two-step process as follows:

1. Formation of a very thin SiC layer by the direct reaction between SiO(g) and diamond.
2. Deposition of SiC on a thin SiC layer by reaction (7).

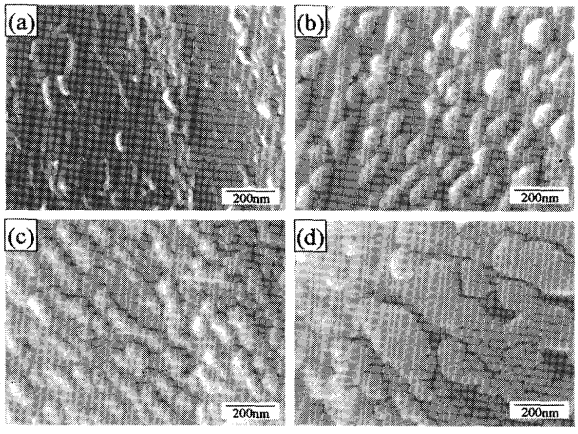

Fig. 5 SEM images of the SiC-coated diamond prepared at 1350 ℃ for (a) 1 min, (b) 15 min, (c) 30 min, and (d) 90 min.

2.3 SiC coating on carbon nanotubes

Multi-walled carbon nanotubes (MWCNTs) are coated with SiC because MWCNTs are more useful as reinforcements and cost effective than single-walled carbon nanotubes (SWCNTs). The surfaces of MWCNTs' are covered with the SiC granules in the same way as for the SiC-coated diamond particles. The size of SiC granules is influenced by the coating temperature and

time. It is less than 50 nm for the sample treated at 1150 ℃ for 15 min, while about 150 nm at 1550 ℃ for 45 min. Therefore, the size of SiC granules can be controlled by adjusting the coating conditions.

Figure 6 shows a high resolution TEM photograph at the interface between the SiC coating and MWCNTs, which was treated at 1350 ℃ for 15 min. The (111) plane of β-SiC and (002) plane of MWCNTs are clearly observed in the image. Some parts in MWCNTs at the vicinity of the interface with β-SiC show an amorphous structure. The measured angle between (111) plane of β-SiC and (002) plane of MWCNTs as shown in Fig. 6 is 66～71°. This angle matches closely with the angle between two different (111) planes of β-SiC (70.5°). These crystallographic relations suggest that the (111) plane of β-SiC is formed epitaxially on (002) plane of MWCNTs and grown toward the <111> direction.

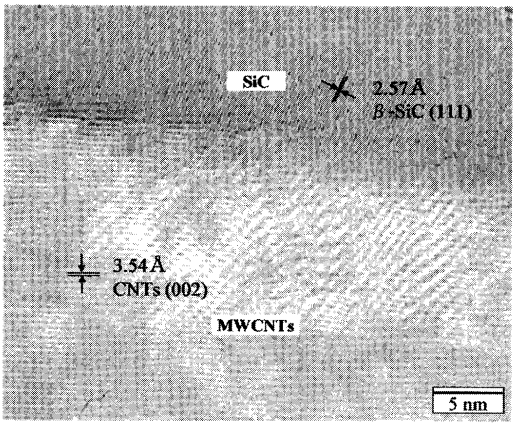

Fig. 6 High resolution TEM image of the SiC-coated MWCNTs prepared at 1350 ℃ for 15 min.

Two types of assembly were used for the SiC coating to investigate the growth mechanism of the SiC layer. In the first method, the SiO powders are set on the bottom of an alumina crucible and MWCNTs are placed upon SiO powders via a carbon felt, as shown in Fig. 7 (a). In the second method, an alumina plate with a center hole is used instead of the carbon felt to separate the MWCNTs from SiO powders, as shown in Fig. 7 (b). These assemblies are covered with an alumina lid to keep the SiO gas pressure inside the crucible, and heated at temperatures between 1250～1550℃ in a vacuum of about 0.03 Pa for 15 min and 30 min.

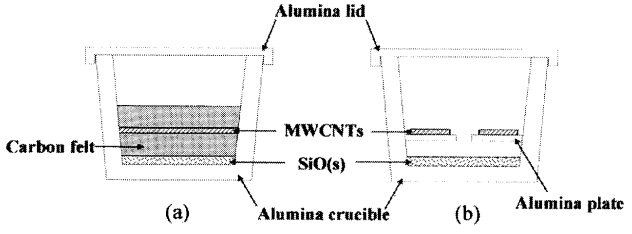

Fig. 7 Assemblies for the SiC coating of MWCNTs with carbon source (a), and without carbon source (b).

Figure 8 (i) and (ii) show the XRD patterns of MWCNTs treated at various temperatures for 15 min. The diffraction peaks of β-SiC appear in all samples. For the samples treated in assembly (a), the peak of MWCNTs exists at 26.2°(2θ) which arises from the (002) graphite layers. However, the peak intensity is very small for the sample treated at 1450 ℃ in assembly (b). The peak of MWCNTs disappears when the sample is treated at 1550 ℃. Above 1450 ℃, the MWCNTs are converted to SiC in assembly (b). Figure 8 (iii) and (iv) show XRD patterns for samples treated at various temperatures for 30 min. Both peaks of β-SiC and MWCNTs exist in assembly (a).

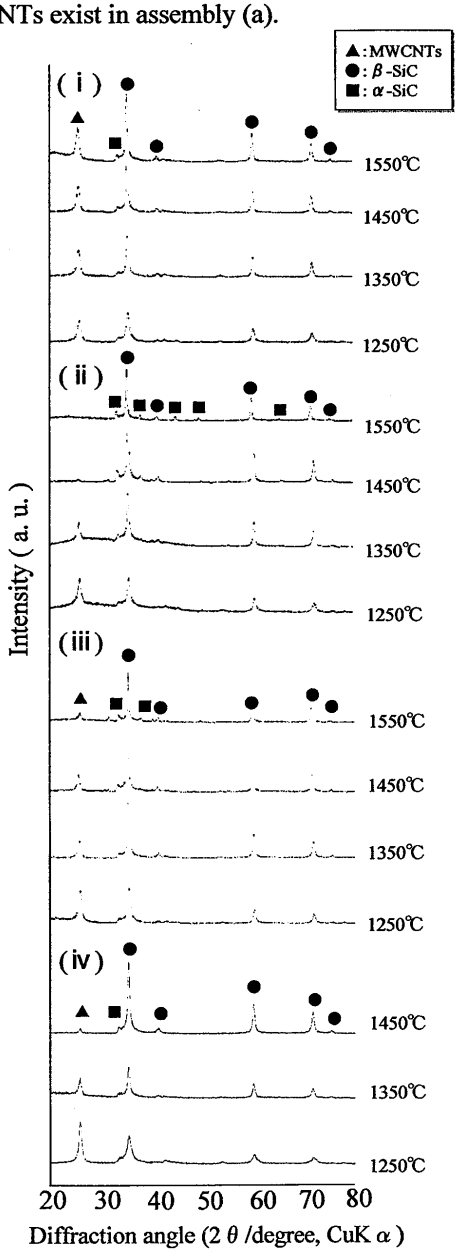

Fig. 8 XRD patterns of the SiC-coated MWCNTs prepared with carbon source (i), and without carbon source (ii) for 15 min, and with carbon source (iii) and without carbon source (iv) for 30 min at various coating temperatures.

However, the sample volatizes away when treated at 1550℃ for 30 min in assembly (b). SiC is oxidized actively under a low oxygen potential at elevated temperature by a reaction called "active-oxidation" following the reaction (3). In this case, the oxidation occurs continuously and SiC is decomposed to SiO(g) and CO(g). The degree of vacuum in the furnace is ~ 0.03 Pa. This coating condition at 1550 ℃ belongs to the active-oxidation region as reported by Naslain et al[37].

In assembly (a), the carbon felt would be oxidized by the following reactions

$$C(s) + O_2(g) = CO_2(g) \quad (9)$$

$$C(s) + 1/2\ O_2(g) = CO(g) \quad (10)$$

A reducing atmosphere with very low oxygen content may not lead to a significant active-oxidation reaction for SiC. Since the treatment for 30 min appears to be ineffective for forming a good SiC layer on MWCNTs, the SiC coated samples prepared for 15 min were utilized to investigate the coating mechanism.

There are some granules on the surfaces of MWCNTs coated in assembly (a). On the other hand, the surfaces of the SiC-coated MWCNTs prepared in assembly (b) are smooth. These morphological differences in SiC coatings suggest that the formation process of the SiC layer is different. Reaction (7) would proceed when there is a rapid decrease in the partial pressure of $CO_2(g)$. Because there is carbon felt in the crucible in assembly (a), $CO_2(g)$ is converted to CO(g) by reaction (8). The CO(g) generated by this reaction will be supplied for reaction (7). In assembly (b), it is difficult to promote reaction (8) because no extra carbon source exists in the crucible. In this case, the surfaces of MWCNTs react directly with SiO(g) and convert to SiC by reaction (2).

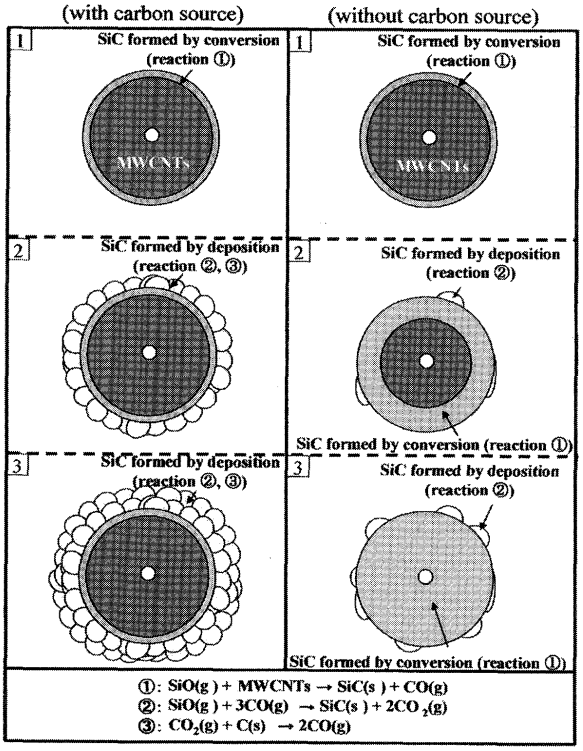

Fig. 9 Growth models of SiC layer on MWCNTs.

From the above results, the growth model of the SiC formation on MWCNTs can be proposed as illustrated in Fig. 9. The growth of SiC is influenced by the existence of the carbon source in the crucible. In the early stage of the reaction, SiO(g) reaches the surface of MWCNTs and forms a thin SiC layer due to reaction (2). This stage needs no carbon source. In assembly (a), SiC granules are deposited on the thin SiC layer by reaction (7). This reaction continues until the SiO(s) is consumed because the partial pressure of $CO_2(g)$ is decreased by reaction (8). The generation of CO(g) by reaction (8) would control reaction (7). MWCNTs can remain after the SiC coating in assembly (a).

In assembly (b), the reaction (2) is promoted and MWCNTs are converted to SiC. It is inferred that MWCNTs are changed to SiC nano-rods by reaction (2) because the diffraction peaks of MWCNTs are not observed on XRD patterns of the sample which is prepared at 1550 ℃ for 15 min. A small amount of nanometer scale SiC granules are deposited by reaction (7) even in assembly (b). In this case, the MWCNTs are considered to play the role of carbon source.

2.4 Oxidation resistance

Figure 10 shows starting temperatures of oxidation for SiC-coated diamond particles depending on the coating time and temperature. The coating at 1350 ℃ shows superior oxidation resistance. When the total coating time is 90 min (30 min coating repeated three times), the starting temperature of oxidation reaches about 950 ℃, which is 400 ℃ higher than that of diamond without SiC coating. Even for diamond particles treated only for 1 min at 1350 ℃, no oxidation starts below 750 ℃. This result suggests the existence of a thin SiC layer on the entire surface of diamond. The thickness of this SiC layer is estimated to be about 15 nm by interpolating the linear

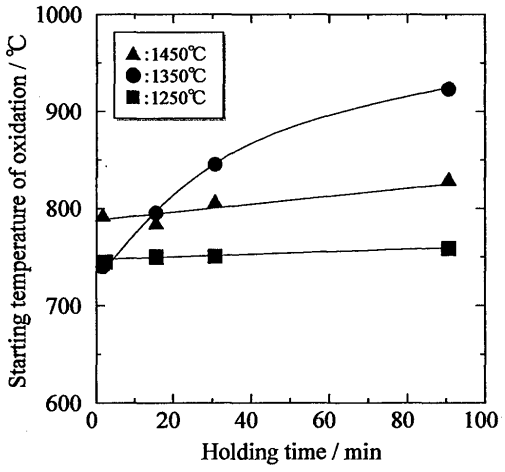

Fig. 10 Starting temperature of oxidation for the SiC-coated diamond particles.

relation between the thickness of the SiC layer and the holding time at 1350 ℃. The diamond surface is converted to SiC by the reaction-diffusion of Si into diamond. Other coatings at 1250 ℃ and 1450 ℃ show lower oxidation resistance. It is reported that the transformation of diamond to graphite and the generation of cracks in diamond starts at over 1400 ℃[41]. The coating at 1250 ℃ for 90 min exhibits no improvement against oxidation compared to the coating at the same temperature for 1 min.

The oxidation durability of SiC-coated diamond particles treated at 1350 ℃ for 30 min and 90 min is evaluated at 700 ℃ in an air flow of 50 ml/min. The uncoated diamond particles show a rapid weight loss, whereas the SiC coated diamond particles treated for 90 min maintain over 70 % of their weight after oxidation for 5 h.

It is easy to form SiC nanorods in assembly as shown in Fig. 7 (b). The SiC nanorod must show excellent oxidation resistance. However, the microstructure and superior properties of MWCNTs are lost. Therefore, only the SiC-coated MWCNTs treated in the assembly shown in Fig. 7 (a) for 15 min are evaluated. Figure 11 shows the TG curves for SiC-coated MWCNTs which are heated at 650 ℃ in air. As-received MWCNTs are oxidized completely within 5 min. The remaining mass detected (~2.5 %) is attributed to iron because it is used as a catalyst for the synthesis of MWCNTs. Further heating increases the mass gain probably due to the formation of Fe_2O_3. For the SiC-coated MWCNTs treated at 1550 ℃, about 90 % of mass remains after heating at 650 ℃ for 60 min. The SiC coating at higher temperature provides an improved oxidation resistance.

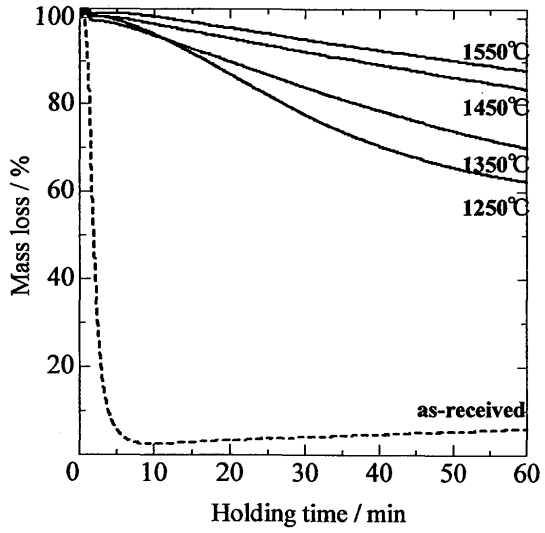

Fig. 11 TG curves for the SiC-coated MWCNTs heated at 650 ℃ in air. The coating was carried out at various temperatures from 1250 ℃ to 1550 ℃.

The morphological change of MWCNTs before and after the oxidation at 650 ℃ for 10 sec is shown in Fig. 12 (a) and (b). A tip of MWCNTs before oxidation is closed with a cap. On the other hand, the cap is removed after oxidation for 10 sec. It is reported that the cap is not resistant to chemical reactions because it has a pentagonal shape[42]. When the cap is lost, oxygen can enter the interplanar spaces between [002] planes of MWCNTs. Such planes of carbon atoms are bonded by Van der Waals forces. It is well known that the (002) plane of graphite has a higher oxidation rate than other planes. Therefore, the tip of MWCNTs is very important to prevent oxidation of MWCNTs. For the sample coated at 1350 ℃ for 15 min, the surface and cap are covered with tiny SiC granules (Fig. 12 (c)). The cap is held and about 70 % of the mass remains after oxidation at 650 ℃ for 1h (Fig. 12 (d)).

A relatively strong (002) peak of MWCNTs remains on the XRD pattern even after oxidation tests. The oxidation rate must be controlled by the diffusion of oxygen through the SiC layer. The crystalline size of SiC

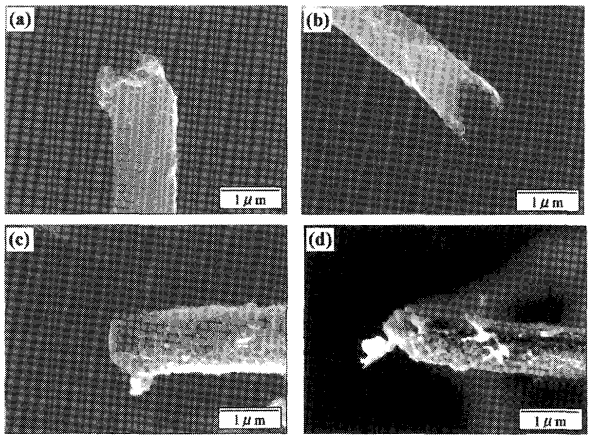

Fig. 12 SEM photographs of MWCNTs and SiC-coated MWCNTs. (a): as-received MWCNTs, (b): MWCNTs oxidized at 650 ℃ for 10 second, (c): SiC-coated MWCNTs, (d): SiC-coated MWCNTs oxidized at 650 ℃ for 60 min.

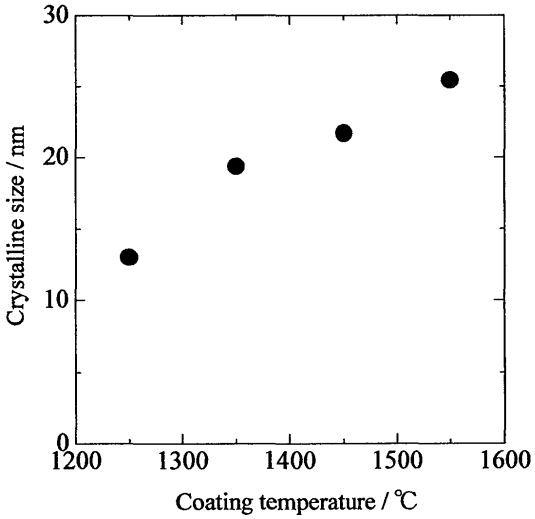

Fig. 13 Relation between coating temperature and apparent crystalline size of SiC.

can be estimated using the Scherrer's equation for (111) peak of β-SiC and plotted as a function of coating temperature in Fig. 13. The crystalline size of SiC gradually increases from 13 nm to 26 nm with an increase in coating temperature. The higher coating temperature can produce dense and thick SiC layers with larger crystalline size, resulting in a higher oxidation resistance. The shape of the SiC coated MWCNTs is not changed by the oxidation test. No crack or exfoliation is observed on the surface.

3. Application of nanostructured SiC coatings in advanced composites

3.1 Development of SiC-coated diamond/WC-Co composites

Cemented carbide, an alloy made of tungsten carbide (WC) and cobalt (Co), is widely used for cutting tools and wear-resistant tools because of the excellent hardness, strength, toughness, and Young's modulus[43]. Although sintered diamond has extremely high hardness and wear resistance[43], it is costly and limited in size and shape because of the need for using ultra-high-pressure and difficult in machining. Therefore, the composite formation of cemented carbide and diamond under lower pressure is very attractive because new wear resistant tools can be produced with lower cost. However, diamond reacts with cobalt at the sintering temperature of cemented carbide, ~1150 ℃, and converts to graphite. This reaction must be prevented to develop the diamond dispersed cemented carbide.

SiC-coated diamond powders with a particle size of ~8-16 μm are mixed with fine WC and cobalt powders (10 wt% Co) and sintered in a vacuum at 1220 ℃, 30 MPa for 5 min by pulsed-electric current sintering (PECS)[44,45]. The diamond content is 20 vol%. The PECS method enables sintering of materials at a lower temperature and shorter time than the conventional sintering methods because it uses a high pulsed current of 1000-3000 A. This current is sent through the material directly, after placing the material in a graphite mold, under uniaxial loading.

Figure 14 (a) is a SEM micrograph of the polished surface of a SiC-coated diamond dispersed WC-10wt%Co composite. It is well sintered and the diamond particles are uniformly dispersed. The relative density reaches 99.5 %. The dense composite suggests that the SiC layer protects the diamond from attack by molten cobalt and prevents the conversion of diamond surface to graphite. In contrast, when uncoated diamond powders are mixed with WC-Co, well-sintered materials could not be obtained.

Values of Vickers hardness and indentation fracture toughness measured for the WC-Co with and without SiC-coated diamond are compared in Table 1. The Vickers hardness is measured under a 98 N load. The fracture toughness is evaluated under the same load using the indentation fracture method. Both sintered composites show almost the same hardness of ~15.5 GPa. However, the fracture toughness of the diamond dispersed composite was 16.3 MPa · $m^{1/2}$, which is nearly 200 % higher than that of a WC-10wt%Co itself. Because of the extremely high hardness (~110 GPa) and high Young's modulus (~950 GPa) of diamond, the presence of diamond particles are expected to impede the crack propagation. Such an impeding effect against crack propagations is seen in Fig. 14 (b). The lower thermal expansion coefficient (~3×10^{6}/K)[46] than that of the cemented carbide (5.7×10^{6}/K)[47] and high Young's modulus of diamond would produce a high tensile stress around each diamond particle. Such a high tensile stress can further enhance the crack deflection.[48] No increase in hardness of the cemented carbide composite with SiC-coated diamond dispersion could be attributed to weak bonding between the diamond and cemented carbide matrix. The diamond dispersed cemented carbides have a wear resistance ten times higher than that of the conventional cemented carbides. Such products are commercialized as super wear-resistant tools in Japan[49].

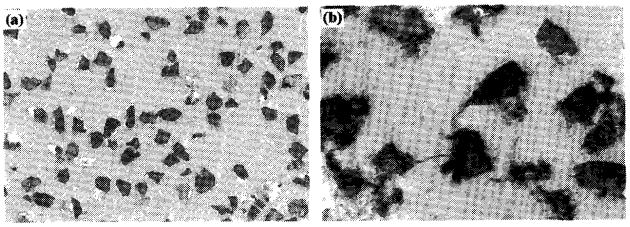

Fig. 14 SEM images of the SiC-coated diamond dispersed cemented carbide composite (a) polished surface, (b) crack propagation.

Table 1 Comparison of Vickers hardness and fracture toughness for cemented carbide sintered with and without SiC-coated diamond particles.

Materials	Vickers hardness (GPa)	Indentation fracture toughness (MPa·$m^{1/2}$)
WC+10wt%Co	15.4	8.7
WC+10wt%Co+20vol% SiC-coated diamond	15.5	16.3

3.2 Development of SiC-coated carbon nanotubes /WC-Co composites

MWCNTs have been tested to reinforce various matrices because they have many unique mechanical and physical properties[14,15]. However, these nanotubes become corroded with metals (such as iron, cobalt, and aluminum) at temperatures above 850 ℃. These shortcomings limit the applications of MWCNTs as nano-reinforcements. The SiC coating can effectively protect the diamond from molten cobalt thus allowing dense SiC-coated diamond dispersed cemented carbide composites to be successfully fabricated at lower pressures. If MWCNTs can be coated with the same SiC layer, more stable MWCNTs would be produced and expected to be used as nano-reinforcements for various matrices. The development of SiC-coated MWCNTs / WC-Co composites has potential to extend both functions of MWCNTs and WC-Co.

SiC-coated MWCNTs or non-coated MWCNTs are dispersed in isopropylalcohol (IPA) using ultrasonic

vibration for 5 min. Then the SiC-coated MWCNTs or non-coated MWCNTs are mixed with fine WC and cobalt powders (10 wt% cobalt) in IPA using plastic balls (10-20 mm in diameter) for 5 h. After ball milling, the IPA solution is evaporated by stirring using an electric heater and then dried at 100 ℃. The MWCNTs are uniformly dispersed without aggregation. The mixed powders are sintered at different temperatures of 950 ℃ ~ 1200 ℃, 30 MPa for 5 min under vacuum using PECS. The content of the SiC-coated MWCNTs is 3 vol%.

The mixed powders of SiC-coated MWCNTs and WC-10wt%Co are charged in a graphite mold and sintered by PECS. The sample is heated from room temperature to sintered temperatures for 20 min. Figure 15 shows the change of relative density of the WC-10wt%Co and the WC-10wt%Co with MWCNTs compacts depending on the sintering temperature. The density of WC-10wt%Co increases with an increase in sintering temperature and reaches nearly 100 % at 1150 ℃. On the other hand, the composites of WC-10wt%Co with MWCNTs are fully sintered at 1050 ℃, which is 100 ℃ lower than the sintering temperature of WC-10wt%Co itself. The resistance heating of MWCNTs is capable of accelerating the sintering process.

The microhardness of the WC-10wt%Co compact increases by incorporating SiC-coated MWCNTs except for the coating at above 1450 ℃, as shown in Fig. 16. The microhardness is measured under a 19.6 N load. It is reasonable to assume that the hardness is probably enhanced by the elastic recovery of MWCNTs. The increase of microhardness by incorporating non-coated MWCNTs is lower than that by SiC-coated MWCNTs. This difference of hardness may be due to the corrosion of non-coated MWCNTs with molten Co and poor adhesion with the matrix as suggested by Laurent et al.[25].

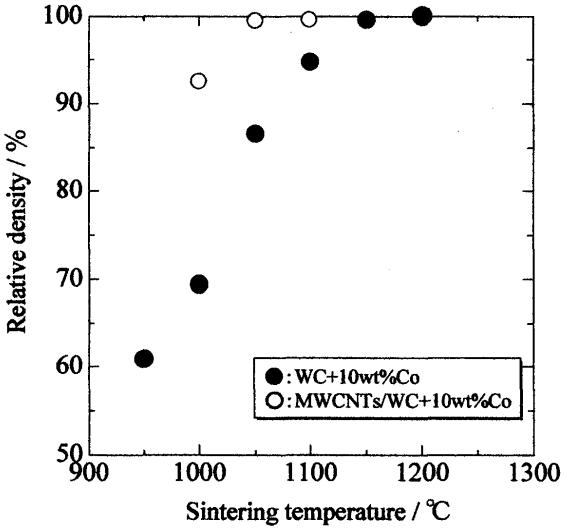

Fig. 15 Relation between relative density of WC-10wt%Co and sintering temperature.

The presence of SiC coating overcomes these problems because SiC is chemically stable and the SiC granules can provide an anchor effect. The lower hardness obtained when SiC-coated MWCNTs prepared at over 1450 ℃ are used for reinforcements could be attributed to the strength degradation of MWCNTs as a result of high coating temperatures.

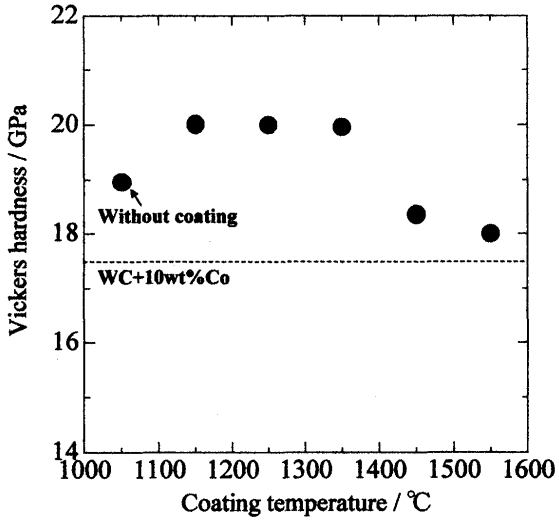

Fig. 16 Relation between microhardness of the WC-10wt% Co compacts with MWCNTs, SiC-coated MWCNTs, and without MWCNTs and coating temperature.

3.3 Development of SiC-coated carbon nanotubes/SiC composites

SiC has high heat and oxidation resistance. Therefore, various applications relating to space developments and efficient power generators are expected. However, the low reliability due to the brittle nature of SiC is a critical problem. MWCNTs may be one of good candidates to reinforce the SiC matrix if the original strength of MWCNTs is maintained. The SiC coating is expected to improve the weak adhesion between MWCNTs and SiC matrix.

The SiC-coated MWCNTs or uncoated MWCNTs are dispersed in isopropyl alcohol (IPA) using ultrasonic vibration for 5 min. The SiC-coated MWCNTs or uncoated MWCNTs are then mixed with nanometer-sized SiC (mean diameter of 30 nm) and B_4C (mean diameter of 240 nm) powders in IPA using ultrasonic vibration for 10 min. The B_4C is added at 2 wt% as a sintering aid. After the mixing, the IPA solution is evaporated and the mixed powders are dried at 100 ℃. The MWCNTs are uniformly dispersed without aggregation. The mixed powders are sintered at 1800 ℃, 40 MPa for 5 min under a vacuum by means of PECS. The content of the SiC-coated MWCNTs is varied between 1-5 vol%.

The microhardness of the SiC compact measured under a 19.6 N load increases by incorporating SiC-coated MWCNTs, as shown in Fig. 17. The hardness reaches 30.6 GPa for the content of 5 vol% SiC-coated MWCNTs. This high hardness is considered as an apparent value due

to the elastic recovery of the indentation after loading. This interesting phenomenon is discussed later. On the other hand, the increment of hardness by incorporating uncoated MWCNTs is very low compared with incorporating SiC-coated MWCNTs. This behavior may be due to the poor adhesion with the matrix. The SiC coating acts as an adhesive to the SiC matrix and the SiC granules provide an anchor effect. The relatively lower hardness is obtained when SiC-coated MWCNTs prepared at over 1250 ℃ are used for reinforcements. It is believed that the high coating temperature causes the strength degradation of MWCNTs due to the conversion of MWCNTs to SiC. Figure 18 shows the values of fracture toughness measured under a 19.6 N load. The toughness increases to 5.4 MPa·$m^{1/2}$ by the dispersion of SiC-coated MWCNTs, although the data are quite scattered. The results are attributed to the improvement of the adhesion between the MWCNTs/SiC matrix and the SiC coating. The hardness of the monolithic SiC and the uncoated MWCNTs dispersed SiC composite are not changed in relation with the indentation load, while that of the SiC-coated MWCNTs/SiC composite increases up to 34.3 GPa when the hardness test is carried out under a 9.8 N load. The fracture toughness has a tendency to increase depending on the decrease of the indentation load. These results suggest that uncoated MWCNTs do not act as reinforcements for the SiC matrix due to a weak interfacial adhesion between the surface of MWCNTs/SiC matrix.

Figure 19 shows the SEM and three-dimensional (3D) images of indentation prints marked by the hardness test under a 19.8 N. The 3D images are composed in the same scale to compare the shape of indentation prints. These images are synthesized with signals of secondary electrons using four detectors in the 3D-SEM equipment. The indentation print of the monolithic SiC ceramic is very sharp reflecting a square pyramidal shape of Vickers hardness tester. The cracks propagate outward from each corner of the indent. The MWCNTs/SiC composite shows somewhat similar fractography. On the other hand, the indentation print and the crack propagation of the SiC-coated MWCNTs/SiC composite are very indistinct and the square pyramidal print cannot be observed in the 3D image. However, the lateral sides of the indent indicate an elastic deformation. It is difficult to understand why such a high hardness of 34.3 GPa is obtained by incorporating only 5 vol% of MWCNTs into the SiC matrix. If we suppose that the SiC-coated MWCNTs are tough and exhibit an excellent load transformation effect, the elastic recovery of the indentation print would occur and show high hardness apparently.

SEM images of the fractured surfaces of a monolithic SiC ceramic, uncoated MWCNTs/SiC, and SiC-coated MWCNTs/SiC are shown in Fig. 20. All samples are dense and pore-free. For the uncoated MWCNTs/SiC composite, pulled-outs of MWCNTs are easily seen compared with that of the SiC-coated MWCNTs/SiC composite. These morphological differences of the fractured surface indicate that SiC layers on MWCNTs should improve the weak adhesion between MWCNTs and the SiC matrix.

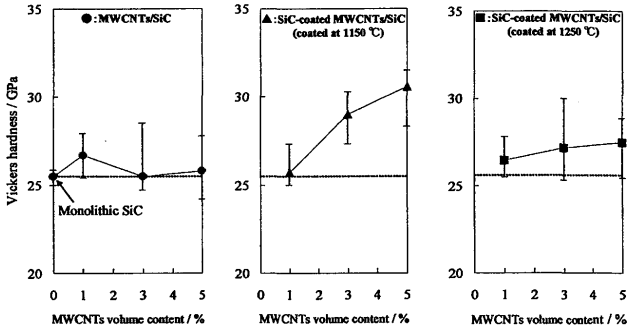

Fig. 17 Relation between microhardness and MWCNTs content.

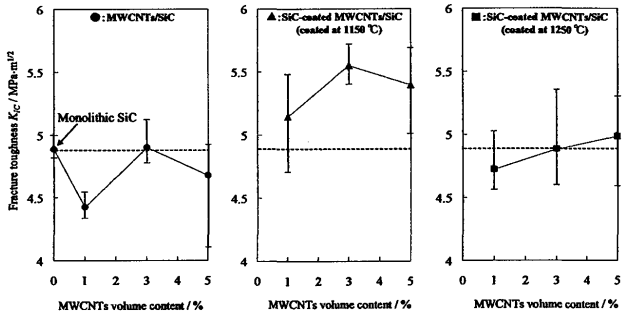

Fig. 18 Relation between fracture toughness and MWCNTs content.

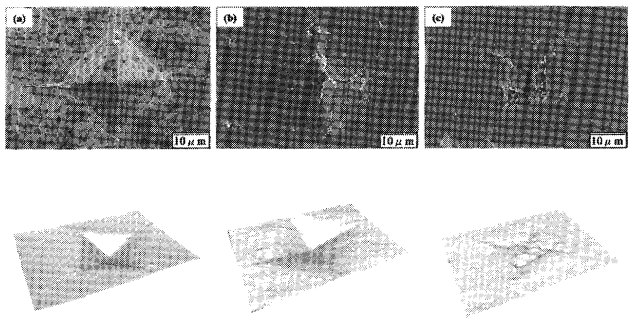

Fig. 19 SEM and 3D images of the indentation: (a) monolithic SiC, (b) MWCNTs/SiC composite, (c) SiC-coated MWCNTs/SiC composite.

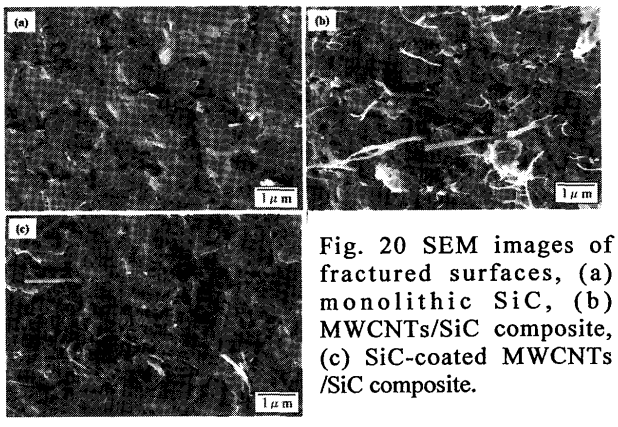

Fig. 20 SEM images of fractured surfaces, (a) monolithic SiC, (b) MWCNTs/SiC composite, (c) SiC-coated MWCNTs /SiC composite.

4. Conclusions

Nanometer sized β-SiC granules are coated on diamond particles and MWCNTs uniformly by a new simple method using SiO. The SiC-coated diamond particles and MWCNTs can act as effective reinforcements to produce new high performance composites. The results can be summarized as follows

(1) The SiC layer grows in two steps. In the first step, a thin SiC layer is formed by the direct reaction between SiO(g) and diamond or MWCNTs. In the second step, nanometer sized SiC granules are deposited on the SiC layer by the vapor phase reaction between SiO(g) and CO(g).

(2) The oxidation resistance of diamond particles and MWCNTs is remarkably improved by the SiC coating.

(3) Dense composites of cemented carbide containing SiC-coated diamond particles can be fabricated without conversion of diamond to graphite. The fracture toughness of the composite is two times higher than that of cemented carbide due to the deflection and blocking effects against crack propagations by the dispersed diamond particles.

(4) The microhardness of WC-10wt%Co increases by the dispersion of SiC-coated MWCNTs. The SiC-coated MWCNTs treated at 1150 ℃ ~ 1350 ℃ can act as nano-reinforcements for WC-Co compacts.

(5) The dispersion of SiC-coated MWCNTs increases the microhardness and fracture toughness of SiC. The SiC coating on MWCNTs at 1150 ℃ is effective in improving the weak adhesion between MWCNTs and the SiC matrix. SiC-coated MWCNTs/SiC composites show an elastic behavior due to the load transformation effect of MWCNTs.

References

1) M. Inagaki, "Carbon Materials", *Solid State Ionics*, 86/88, 833-839 (1996).
2) P. Scharff, "New Carbon Materials for Research and technology", *Carbon*, 36, 481-486 (1998).
3) M.S. Dresselhaus and G. Dresselhaus, "Nanotechnology in Carbon Materials", *Nanostructured Materials*, 9, 33-42 (1997).
4) P. Calvert, "Nanotube Composites-a Recipe for Strength", *Nature*, 399, 210-211 (1999).
5) M.M.J Treacy, T.W. Ebbesen, J.M. Gibson, "Exceptionally High Young's Modulus Observed for Individual Carbon Nanotubes", *Nature*, 381, 678-680 (1996).
6) E.W. Wong, P.E. Sheehan, C.M. Lieber, "Nanobeam Mechanics: Elasticity, Strength, and Toughness of Nanorods and Nanotubes", *Science*, 277, 1971-1975 (1997).
7) Service RF, "Materials Science: Superstrong Nanotubes Show They Are Smart, Too", *Science*, 281, 940-942 (1998).
8) J.P. Salvetat, J.M. Bonard, H.K. Tomson, A.J. Kulik, L. Forro, W. Benoit, L. Zuppiroli, "Mechanical Properties of Carbon Nanotubes", *Appl Phys A*, 69, 255-260 (1999).
9) M.R. Falvo, C.J. Clary, R.M. Taylor, V. Chi, F.P. Brooks, S. Washburn, R. Superfine, "Bending and Buckling of Carbon Nanotubes Under Large Strain", *Nature*, 389, 582-584 (1997).
10) S. Frank, P. Poncharal, Z.L. Wang, W.A. de Heer, "Carbon Nanotube Quantum Resistors", *Science*, 280, 1744-1746 (1998).
11) A. Batchtold, C. Strunk, J.P. Salvetant, J.M. Bonard, L. Forro, T. Nussbaumer, C. Schonenberger, "Aharonov-Bohm Oscillations in Carbon Nanotubes", *Nature*, 397, 673-675 (1999).
12) S.J. Trans, A.R.M. Verschueren, C. Dekker, "Room-temperature Transistor Based on A Single Carbon Nanotube", *Nature*, 393, 49-52 (1998).
13) J. Kong, N.R. Franklin, C.W. Zhou, M.G. Chapline, S. Peng, K.J. Cho, H.J. Dai, "Nanotube Molecular Wires as Chemical Sensors", *Science*, 287, 622-625 (2000).
14) T. Kuzumaki, O. Ujiie, H. Ichinose, K. Ito, "Mechanical Characteristics and Preparation of Carbon Nanotube Fiber-reinforced Ti Composite", *Adv Eng Mater*, 2(7), 416-418 (2000).
15) K.T. Lao, D. Hui, "Effectiveness of Using Carbon Nanotubes as Nano-reinforcements for Advanced Composite Structures", *Carbon*, 40, 1605-1606 (2002).
16) J. W. Fergus and W. L. Worrell, "Silicon-Carbide /Boron-containing Coatings for the Oxidation Protection of Graphite", *Carbon*, 4, 537-543 (1995).
17) H. Hatta, T. Aoki, Y. Kogo, and T. Yarii, "High-temperature Oxidation Behavior of SiC-coated Carbon Fiber-reinforced Carbon Matrix Composites", *Composites: Part A*, 30, 515-520 (1999).
18) L. Cheng, Y. Xu, L. Zhang, and X. Luan, "Oxidation and Defect Control of CVD SiC Coating on Three-dimensional C/SiC Composites", *Carbon*, 40, 2229-2234 (2002).
19) J. A. Costello and R. E. Tressler, "Oxidation of Silicon Carbide Crystals and Ceramics: I In Dry Oxygen", *J. Am. Ceram. Soc.*, 69, 674-681 (1986).
20) K. L. Luthra, "Some New Perspectives on Oxidation of Silicon Carbide and Silicon Nitride", *J. Am. Ceram. Soc.*, 74, 1095-1103 (1991).
21) N. S. Jacobson, "Corrosion of Silicon-based Ceramics in Combustion Environments", *J. Am. Ceram. Soc.*, 76, 3-28 (1993).
22) T. Shimoo, Y. Morisada, and K. Okamura, "Oxidation Behavior of Si-C-O Fibers (Nicalon) under Oxygen Partial Pressures from 10^2 to 10^5 Pa at 1773 K", *J. Am. Ceram. Soc.*, 83, 3049-3056 (2000).
23) T. Shimoo, Y. Morisada, and K. Okamura, "Active-to-passive Oxidation Transition for Polycarbosilane-derived Silicon Carbide Fibers Heated in Ar-O_2 Gas Mixtures", *J. Mater. Sci.*, 37, 1793-1800 (2002).
24) T. Shimoo, Y. Morisada, and K. Okamura, "Oxidation Behavior of Si-M-C-O Fibers under Wide Range of Oxygen Partial Pressures", *J. Mater. Sci.*, 37, 4361-4368 (2002).
25) Ch. Laurent, A. Peigney, O. Dumortier, and A. Rousset, "Carbon Nanotubes-Fe-Alumina Nanocomposites. Part II: Microstructure and Mechanical Properties of the Hot-Pressed Composites", *J. Eur. Ceram. Soc.*, 18, 2005-2013 (1998).
26) E.T. Thostenson, Z.F. Ren, T.W. Chou, "Advances in the Science and Technology of Carbon Nanotubes and their Composites: A Review", *Compos Sci Technol*, 61, 1899-1912 (2001).
27) R.Z. Ma, J. Wu, B.Q. Wei, J. Liang, D.H. Wu, "Processing and Properties of Carbon Nanotubes-nano-SiC Ceramic", *J. Mater Sci*, 33, 5243-5246 (1998).
28) Y. Miyamoto, J. Lin, Y. Yamashita, T. Kashiwagi, O. Yamaguchi, H. Moriguchi, and A. Ikegaya, "Reactive Coating of SiC on Diamond Particles", *Ceramic Engineering and Science Proceedings 21*, 185-192 (2000).

29) Y. Morisada, H. Moriguchi, K. Tsuduki, A. Ikegaya, and Y. Miyamoto, "Growth Mechanism of Nanometer Sized SiC and Oxidation Resistance of SiC-coated Diamond Particles," *J. Am. Ceram. Soc.*, 87, 809-813 (2004).
30) Y. Morisada, H. Moriguchi, K. Tsuduki, A. Ikegaya, and Y. Miyamoto, "Oxidation Resistance of Multiwalled Carbon Nanotubes Coated with Silicon Carbide", *J. Am. Ceram. Soc.*, 87, 804-808 (2004).
31) Y. Miyamoto, T. Kashiwagi, K. Hirota, O. Yamaguchi, H. Moriguchi, K. Tsuduki, and A. Ikegaya, "Fabrication of New Cemented Carbide Containing Diamond Coated with Nanometer-Sized SiC Particles", *J. Am. Ceram. Soc.*, 86, 73-76 (2003).
32) Y. Morisada and Y. Miyamoto, "SiC-coated Carbon Nanotubes and Their Application as Reinforcements for Cemented Carbides," *Materials Science and Engineering A*, 381, 57-61 (2004).
33) Y. Morisada, Y. Takaura, K. Hirota, O. Yamaguchi, and Y. Miyamoto, "Mechanical Properties of SiC Composites Incorporating SiC-coated Multi-walled Carbon Nanotubes", *J. Am. Ceram. Soc.*, to have been submitted.
34) M. Miyata, Y. Sawai, Y. Yasutomi, and T. Kanai, "Microstructure of Si_3N_4-SiC Ceramics Prepared from Si-SiO-C Mixed Powder", *J. Ceram. Socd. Japan,* 106, 815-819 (1998).
35) K. Fujii, J. Nakano and M. Shindo, "Evaluation of Characteristic Properties of a Newly Developed Graphite Material with a SiC/C Composition Gradient", Proceedings of the 3rd International Symposium on Structural and Functionally Gradient Materials, Edited. By B. Ilschner and N. Cherradi, Lausanne, 541-547 (1995).
36) T. Shimoo, F. Mizutaki, S. Ando, and H. Kimura, "Mechanism of Formation of SiC by Reaction of SiO with Graphite and CO", *J. Japan Inst. Metals,* 52, 279-287 (1988).
37) B. Schneider, A. Guette, R. Naslain, M. Cataldi, and A. Costeaclde, "A Theoretical and Experimental Approach to the Active-to-passive Transition in the Oxidation of Silicon Carbide", *J. Mater. Sci.*, 33, 535-547 (1998).
38) T. Narushima, T. Goto, Y. Iguchi, and T. Hirai, "High-Temperature Active Oxidation of Chemically Vapor-Deposited Silicon Carbide in an Ar-O_2 Atmosphere", *J. Am. Ceram. Soc.*, 74, 2583-2586 (1991).
39) T. Shimoo, H. Takeuti, and K. Okamura, "Thermal Stability of Polycarbosilane-Derived Silicon Carbide Fibers under Reduced Pressures", *J. Am. Ceram. Soc.*, 84, 566-70 (2001).
40) T. Shimoo, Y. Morisada, and K. Okamura, "Suppression of Active Oxidation of Polycarbosilane-Derived Silicon Carbide Fibers by Preoxidation at High Oxygen Pressure", *J. Am. Ceram. Soc.*, 86, 838-845 (2003).
41) B. G. Gargin, "Thermal Destruction of Synthesis Diamond", *Advanced Materials*, 2, 17-20 (1982).
42) Y. Saito, R. Mizushima, and K. Hata, "Field Ion Microscopy of Multiwall Carbon Nanotubes: Observation of Pentagons and Cap Breakage under High Electric Field", *Surface Science,* 499, 119-123 (2002).
43) H. Suzuki, *Cemented Carbide and Sintered Hard Material*, Tokyo, Maruzen (1986).
44) M. Omori, "Sintering, Consolidation, Reaction and Crystal Growth by the Spark Plasma System (SPS)", *Materials Science and Engineering A*, 287, 183-188 (2000).
45) T. Takeuchi, M. Tabuchi, I. Kondoh, N. Tamari, and H. Kageyama, "Synthesis of Dense Lead Titanate Ceramics with Submicrometer Grains by Spark Plasma Sintering", *J. Am. Ceram. Soc.*, 83, 541-544 (2000).
46) Y. S. Touloukian, R. K. Kirby, R. E. Taylor, and T. Y. R. Lee, p. 19 in Thermophysical Properties of Matter, Vol. 13, *Thermal Expansion.* IFI/Plenum, New York (1977).
47) G. S. Upadhyaya, "Materials Science of Cemented Carbides: An Overview", *Mater. Des.*, 22, 483-489 (2001).
48) K. T. Faber and A. G. Evans, "Crack Deflection Process- I . Theory, and II . Experiment", *Acta Metall.*, 31, 565-584 (1983).
49) H. Moriguchi, K. Tsuzuki, H. Itozaki, A. Ikegaya, K. Hagiwara, M. Takasaki, Y. Yanase, and T. Fukuhara, "Fabrication and Applications High-toughness, Highly Wear-resistant Diamond- and cBN- dispersed Cemented Carbide", *Sei Technical Review*, 51, 121-125 (2001).